Mechanical Study of a Superconducting 28-GHz Ion Source Magnet for FRIB

Heng Pan, Diego Arbelaez, Helene Felice, Aurelio. R. Hafalia, Thomas Lipton, Scott Myers, Guillaume Machicoane, Mykola Omelayenko, Soren Prestemon, Eduard Pozdeyev, Etienne Rochepault, and Xing Rao

***Abstract*—The superconducting electron cyclotron resonance (ECR) source magnet for the facility for rare isotope beams at Michigan State University was designed and built by the Superconducting Magnet Group at Lawrence Berkeley National Laboratory (LBNL) in 2017. The 28 GHz NbTi ion source magnet features a sextupole-in-solenoids configuration which is comparable to the VENUS ECR magnet operated at LBNL. However, the mechanical design of this magnet utilizes a shell-based support structure which allows fine adjustments to the sextupole preload and reversibility of the magnet assembly process. The magnet has been assembled and tested to operational currents at LBNL. This paper describes the mechanical analyses performed to estimate the sextupole's and solenoids' preloads. We will report on the 3-D finite element analysis during room temperature assembly, cool-down, and magnet excitation, and then describe the magnet preload operations. Finally, we will describe the performance of the support structure during the quench training.**

I. Introduction

The Facility for Rare Isotope Beams (FRIB) at Michigan State University (MSU) is being developed to provide intense beams of rare isotopes for research in nuclear physics, nuclear astrophysics, and the study of fundamental interactions. In collaboration with MSU, Lawrence Berkeley National Laboratory (LBNL) designed and fabricated a high performance superconducting Electron Cyclotron Resonance (ECR) ion source magnet, capable of operating at 28 GHz [1], [2], with similar performance specifications as for the VENUS [3] ion source. Given the demonstrated reliable performance of VENUS, the main magnetic parameters closely match those of VENUS, and the "sextupole-in-solenoids" assembly configuration is preserved [4]. To avoid conductor stick-slip motion under Lorentz forces, the solenoids and sextuples require precise control of the coil pre-load. The solenoid preload is applied by winding tension, and slip planes are used in this magnet to reduce the possibility of stick-slip motion at the solenoid-mandrel interfaces. The initial sextupole radial preload is applied by the "bladder and key" concept [5], with the solenoids mandrel being used as the support structure for the sextupole assembly. This "shell-based" structure and "bladder-and-key" technology are being utilized in the development of the future HiLumi LHC Nb_3Sn quadrupole magnets [6], [7]. The "bladder-and-key" concept uses water-inflatable metal bladders (removed after assembly) and load keys inside the structure to provide initial preload to the coil structure at room temperature. The final pre-load is achieved during the cool-down phase, when the tensioned shell structure (which is the aluminum mandrel in this case) compresses the structure components, due to its high thermal contraction.

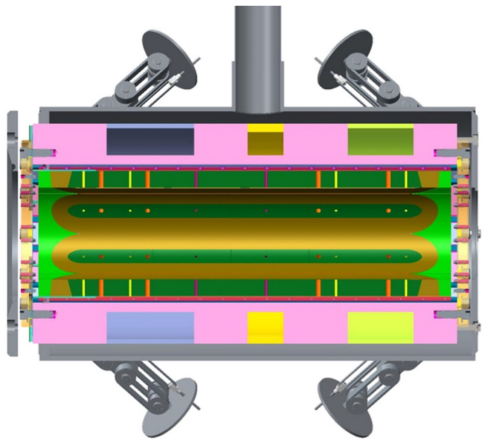

Fig. 1. Cross section of the FRIB ECR magnet.

The FRIB ECR magnet was assembled and pre-loaded at LBNL in 2016, and tested in 2017. The magnet achieved all the specifications. Mechanically, the magnet stress level derived from the strain gauges is within the target range after cool-down, and the coil strains do not show signs of unloading.

This paper is focused on the analysis of the mechanical behavior of the magnet structure. We present the finite element analysis from assembly to excitation; report on the magnet assembly and preload process, and mechanical performance in magnet final training tests.

This work was supported by the U.S. Department of Energy, Office of Science under Contract DE-AC02-05CH11231 and under Cooperative Agreement DE-SC0000661. *(Corresponding author: Heng Pan.)*

H. Pan, D. Arbelaez, A. R. Hafalia, T. Lipton, S. Myers, and S. Prestemon are with Lawrence Berkeley Laboratory, Berkeley, CA 94720 USA (e-mail: hengpan@lbl.gov).

H. Felice and E. Rochepault are with the French Atomic Energy Commission 91400, Saclay France.

G. Machicoane, M. Omelayenko, E. Pozdeyev, and X. Rao are with the Facility for Rare Isotope Beams, Michigan State University, East Lansing, MI 48824 USA.

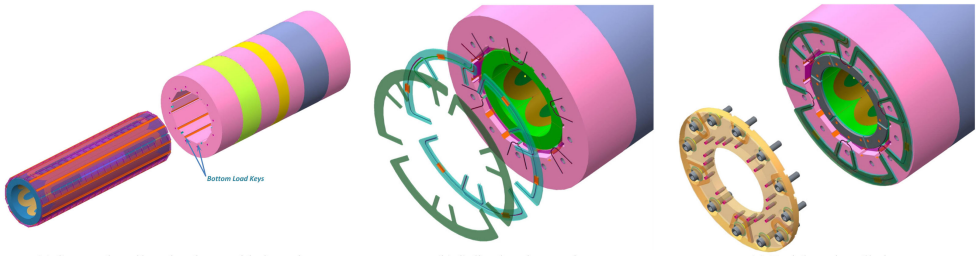

(a).Sextupole coil pack subassembly insertion (b).Splice box integration (c).Endplates installation

Fig. 2. Schematic of magnet assembly.

TABLE I
FRIB ECR MAGNET SOLENOIDS PARAMETERS

Parameters	Injection	Middle	Extraction
Inner/ Outer radius (mm)	170/229.46	170/220.98	170/229.46
Length (mm)	190	78	136
Number of turns per layer/ layers	112/56	46/48	80/56
Nominal current (A)	233	-155	152
Peak field at nominal (T)	6.15	-3.4	4.1
Inductance (H)	14.02	2.5	8.1

TABLE II
FRIB ECR MAGNET SEXTUPOLE PARAMETERS

Inner/ Outer radius (mm)	100/136.9
Nominal end-shoe to end-shoe Length (mm)	896
Number of turns	650
Nominal current (A)	450
Peak field at nominal (T)	6.8
Lorentz Forces on straight section at nominal	
F_r/F_θ on top coil (positive in y direction in Fig .3, kN)	220/-202
F_r/F_θ on bottom coil (negative in y direction in Fig. 3, kN)	240/215

II. MAGNET PARAMETERS AND ASSEMBLY

The FRIB ECR magnet structure (Fig. 1), described in detail in [4] and [8], is comprised of the solenoid-mandrel subassembly and the sextupole coil pack subassembly.

The three solenoids are dry-wound and vacuum impregnated on an aluminum mandrel under winding tension. An external Aluminum banding is wrapped around each solenoid to provide additional radial preload. In addition to the radial forces, the solenoids are subjected to axial Lorentz forces which tend to separate them. In order to avoid stick-slip at the solenoid/mandrel interfaces, Mylar-Mylar slip planes are introduced to minimize friction and energy dissipation.

The sextupole coil pack features six stainless steel pads separated by open gaps and contained in the aluminum mandrel. Between the pads and the mandrel, there are the channels for the water-pressurized bladders and for the load keys. The sextupole coils are surrounded by the pads forming the sextupole coil-pack subassembly.

The sextupole coil pack subassembly was initially assembled at LBNL. Previous experience has shown the importance of properly matching the load pad inner diameter with the coil outer diameter, since improper matching of the radial surfaces may cause ineffective preload or non-uniform loading on the pole turns. Matching is achieved by shimming the coil radius and mid-planes to match the inner radius of the load pads. These shims are made up of G10 and Kapton sheets in various thicknesses. The Kapton sheets also act as the ground plane insulation. After checking the exposure of pressure sensitive paper, the final shim stack is determined as 0.2 mm G10 bonded to pad inner surface plus 0.13 mm Kapton wrapped on the coil OD. Regarding the mid-plane shim, 0.25 mm G10 sheet is used on each side per coil.

Squareness measurements of the sextupole coil-pad build are performed after torqueing the load pads around the sextupole coils. These measurements determine the load key clearances and the initial shim thickness.

As shown in Fig. 2(a), the sextupole coil pack assembly is ready to be inserted into the mandrel. Two bottom keys are initially placed in the mandrel's key ways, and then the coil pack subassembly is inserted on the bottom load keys; finally, six bladders and the rest load keys are inserted between the pads and the mandrel.

Once the insertion operation completed, all of the sextupole coils are spliced together in the splice box as shown in Fig. 2(b). The splice box consists of G10 base plates with grooves for the route leads, and G10 cover plates. The route leads from sextupole coils are spliced in accordance with the magnet electrical specification. Copper braids are soldered along each routed lead, acting as additional heat sinks, to provide extra thermal stability.

After the splice box is completely assembled, the structural assembly preloaded by bladder and key operations, which is the most important step in the assembly (see Section IV). Then the stainless steel endplates could be installed as the last step of the magnet assembly as seen in Fig. 2(c). The endplates provides axial loading after cool-down through a set of stainless steel bullets. Because most of axial load is from thermal contraction of the mandrel, minimal axial preload is applied on the bullet at room temperature.

III. NUMERICAL ANALYSIS OF THE ASSEMBLY

The complete of the magnet assembly requires the final preload operations at room temperature. Numerical analysis is performed upon the assembled structure to determine the preloads for the assembly.

A. Mechanical Model

A fully parametric FE model is developed in ANSYS (See Fig. 3) for pre-assembly design and preload determination.

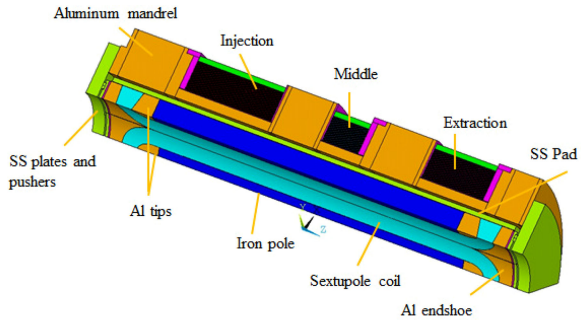

Fig. 3. Sextant 3D model in ANSYS.

TABLE III
FRIB ECR MAGNET MATERIAL PROPERTIES

Material		E [GPa] 293 K/4.2 K	α (293 K -> 4.3K)	$\sigma_{0.2}$ (MPa) 293 K/4.2 K
Sextupole Coil	E_r	38/38	3.48e-3	-
	E_θ	30/30	3.6e-3	
	E_z	75/75	3.2e-3	
Solenoid coil	E_r	45/45	3.4e-3	-
	E_θ	90/90	3.00e-3	
	E_z	60/60	3.4e-3	
Aluminum		70/79	4.2e-3	420 / 555[9]
Iron		213/224	1.97e-3	-
Stainless steel		193/210	2.84e-3	289/375

Elements were generated using a volume sweep of 20-node structural elements (SOLID95). The contact areas between at the assembly interfaces (sextupole/pad, pads/load keys, load key/mandrels, and solenoids/mandrel) were modeled with TARGE170 and CONTA174 elements with asymmetric behavior and augmented Lagrange formulation. All the contacts are bonded inside of the sextupole coil (i.e., coil, pole, end-shoe, and Al tips) to account for the epoxy impregnation. Friction coefficient of 0.2 is used on the other contacts. Derived material properties are listed in Table III. The coil properties are inferred on the basis of rule of weight. The model simulates the key shimming by means of applying contact interference between the load key and the master pad. The interference in the model represents the net shim thickness added in the pre-load process on top of the initial load key shims.

Cyclic symmetry boundary condition is applied at $\pm 30°$ of the solenoids in order to keep the direction of the winding tension consistent at the symmetric planes. Regular symmetry planes are imposed at $\pm 30°$ for the remaining parts. In addition, to constrain the model axially, the axial displacement of the nodes is forced to 0 at $z = 0$ (the middle plane of the Middle solenoid) in the mandrel and pad.

The entire operation process was simulated by the following four primary steps:

1) Solenoids winding with pre-tension.
2) Sextupole key shimming: the shim was applied as the contact interference between load key and solenoid mandrel.
3) Cool-down: the temperature of all solids was changed from 293 K to 4.2 K.
4) Magnetic excitation to nominal currents: Import the coil forces from Opera3D to ANSYS.

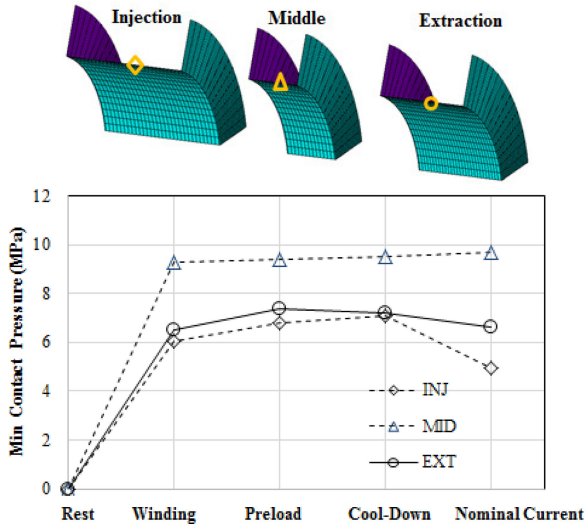

Fig. 4. Simulated contact pressure (MPa) at the solenoids/mandrel interface. The above figure of contact elements of all the three solenoids shows the location of the plots.

B. Numerical Results of Solenoids Assembly

The solenoids were wound under tension on the Aluminum mandrel to maintain compression. The figure of merit for the winding tension is to ensure at least 5 MPa contact pressure at the solenoid/mandrel interface.

The solenoids and reinforcement winding tensions are simulated by imposing initial hoop tension in each layer and employing the element death and birth technique, which suppresses the unwound layers, and reactivates the suppressed elements when they start to be wound.

As shown in Fig. 4, the analysis indicates that the injection coil has the least radial contact pressure after excitation. Because the thermal contraction of the solenoids is less than aluminum mandrel, the contact pressure between solenoids and mandrel will reduce after cool-down; Moreover, the Lorentz force in solenoids reduces the contact pressure as well. The pressure reduction is quite obvious in the Injection and Extraction coil. The contact pressure of the Middle coil does not change due to the least Lorentz force. 5 MPa contact pressure after powering is considered as the minimum. In order to maintain this minimum contact pressure, 60 MPa winding tension is required for all the solenoids.

On the other hand, the solenoid winding tension causes the mandrel inner diameter to move inward radially, giving a wavy shape to the mandrel longitudinally. This inward displacement reduces the load key clearances for the sextupole preload operation. Fig. 5 shows the radial displacement in the key ways of the mandrel after winding. The round marker indicates the radial deformation measured by a straightedge and feeler gauges after winding. The prediction of the model is close to the general shape of the mandrel deformation.

C. Numerical Results of Sextupole Assembly

The sextupole pole turns must be in azimuthal compression along the straight section and in axial compression at the ends

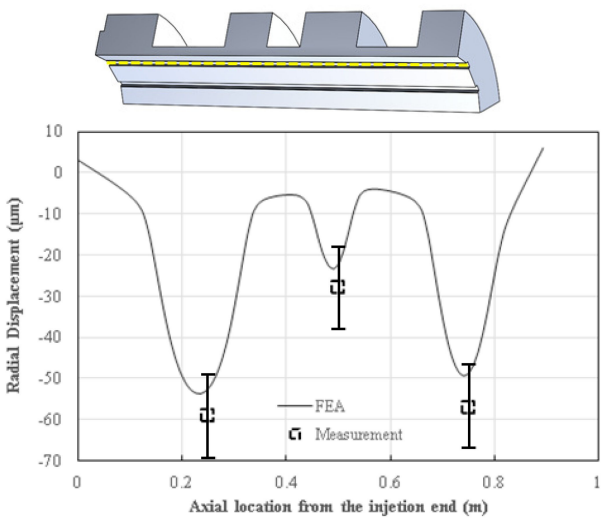

Fig. 5. Radial displacement along the key way (yellow dash line) after winding, error bar is $+/-10$ micron.

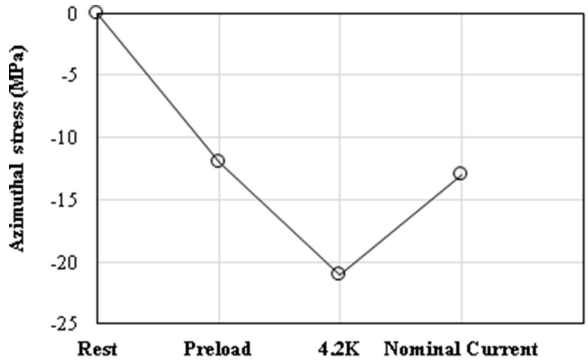

Fig. 6. Minimum azimuthal compressive stress at the coil/pole interface over the major operation steps.

during excitation to minimize conductor motions. The initial preload is achieved at room temperature in the preload operation. Differential thermal contraction of the support structure components during cool-down to the 4.2 K completes the final preload.

The room temperature preload is applied by means of load shims. The goal of the preload is to keep positive contact pressure at the coil/pole interface at all stages of operations.

The analysis for the entire magnet suggests that 0.12∼0.15 mm shim thickness is appropriate according to the FE solutions. The shimmed load key was simulated in the FE model by imposing an interference of shim thickness between load keys and mandrel key slots.

Due to the wavy shape deformation of the mandrel caused by solenoid winding, the azimuthal preload on the sextupole is inhomogeneous longitudinally with relatively strong compression under the solenoids, and weak compression under the sections between solenoids. This improves after cool-down since the aluminum mandrel shrinks more than the solenoids; therefore, reducing the wavy shape deformation of the mandrel at 4.2 K.

Fig. 6 illustrates the minimum azimuthal stress at the coil/pole interface over the various operation steps with shim thickness of 0.12 mm. With this preload level, the azimuthal stress is negative

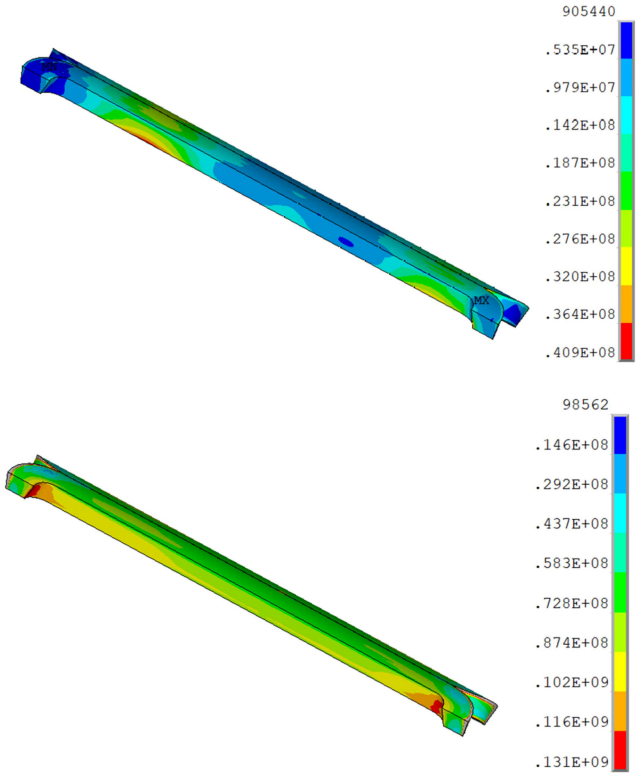

Fig. 7. Von Mises stress (Pa) on sextupole coils (upper: after room temperature preload; below: stress distribution at 4.2 K).

(compressive) everywhere along the coil/pole interface with a minimum compressive stress of 13 MPa at excitation.

The Von Mises stress distribution on sextupole coils after room temperature preload and cool-down is shown in Fig. 7. The peak stress on coil is well below the allowable stress seen in NbTi coils at both room temperature and 4.2 K. Simulation also shows the Von Mises stress in each part of the magnet is lower than the material yield limits at both room and cryogenic temperature.

IV. Magnet Preload at Room Temperature

A. Room Temperature Preload

The magnet preload at room temperature is a critical step in the assembly process, and it requires numerical analysis to determine the appropriate preload level.

In the case of FRIB ECR magnet, the numerical analysis suggests 0.12∼0.15 mm load key shims to for the room temperature preload.

As described in Section II, the bladders are inserted between the pads and the mandrel after the splice box was finished. Fig. 8 shows the schematic of bladders and load keys in the assembly. The bladders are inflated with pressurized water (up to 34 MPa), compressing the coil azimuthally and stretching the mandrel. When the bladders are inflated, gaps open between the load keys and the mandrel for the appropriate shimming (about 0.12–0.15 mm); the bladders are deflated and removed. The shimmed load keys maintain the sextupole in azimuthal compression.

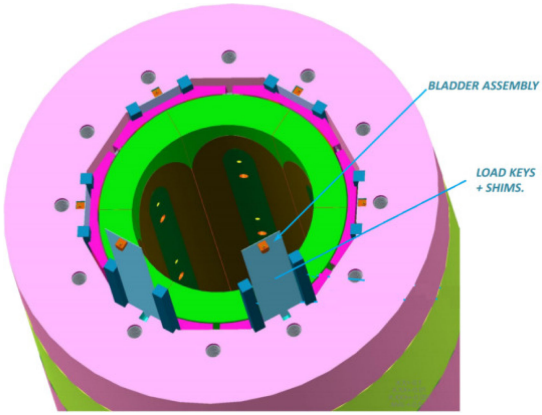

Fig. 8. Schematic of bladders installation.

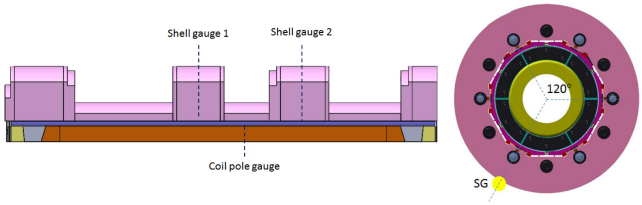

Fig. 9. Strain gauge locations on mandrel and coils.

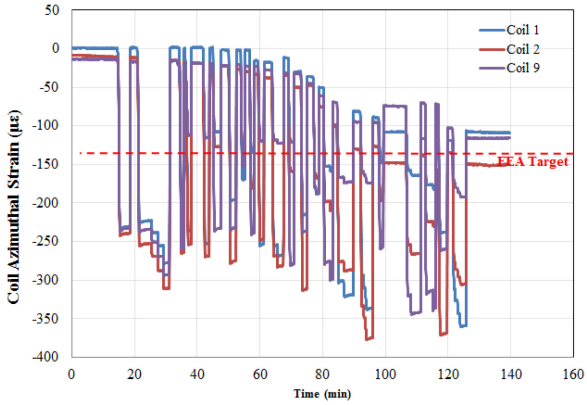

Fig. 10. Strain data of the pole in the azimuthal pre-loading.

The aluminum mandrel and all of the sextupole coils are instrumented with strain gauges mounted on the mandrel and the coil pole piece, which are shown in Fig. 9. During operations through assembly to excitation, strain gauges allow for the measurement of the mandrel tension and coil pole compression. This information is compared with the transfer function determined by the 3D FE model.

Because of the wavy shape deformation of mandrel, the strain on the coil pole and mandrel inner surface is longitudinally inhomogeneous. The section under the middle solenoid is the least loaded area as described in Fig. 4. To be conservative, the coil pole gauges are installed under the center of the middle solenoid, and the mandrel gauges are installed on the outer surface of the mandrel next to the middle solenoid.

Fig. 10 shows the measured azimuthal strain of the coil iron poles. Note that gauges on coil 3, coil 7 and coil 8 were lost in the

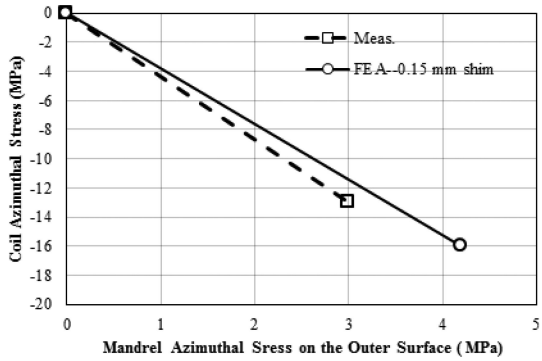

Fig. 11. TF plot of the pole and shell azimuthal stress after pre-loading at room temperature.

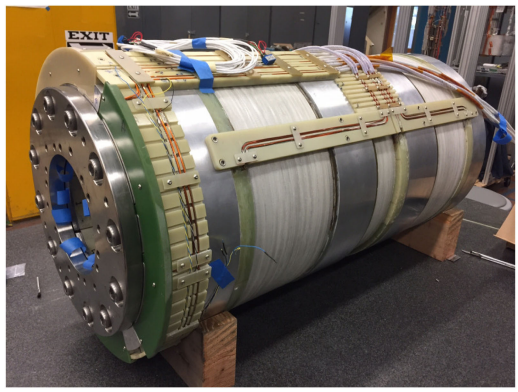

Fig. 12. The finished FRIB ECR magnet.

previous tests. The preload at room temperature was performed at several steps under different bladder pressures. Initially, all six sextants were pressurized at the same time. However, coil azimuthal stress reached ∼100 MPa at bladder pressures above 20 MPa. That is because the layout of the load key and bladders of the pad, the coil got extra bending during the bladder operation to open up a gap for the appropriate shim thickness. In order to maintain the coil stress below 100 MPa, only every other bladder (at 120° apart) was pressurized in the second stage of preloading. In the third stage, bladders of coils across from each other were pressurized. In the final stage, the bladders were pressurized individually to obtain the final preload. The maximum bladder pressure was 31 MPa, corresponding to a net shim thickness of 130 μm. Due to the slight differences on coil size, uneven compression may be applied on each coil and results in the different coil strain. The average strain is used as the indicator of the overall preload.

According to the FE simulations, the pole stress closely matches the coil stress at the pole-turn inner surface. For "bladder and key" structures, a Transfer Function (TF) is used to study the relationship between the shell and the pole stresses [7]. The room temperature preload result for such TF is shown in Fig. 11. The slope of the shell stress and pole stress represents the relationship between the magnet support structure and the coils. The measurement shows a small inconsistency with the FE model, but they are in reasonably good agreement. As seen in Fig. 12, the final assembled magnet was cool-down to 4.2 K. The coil

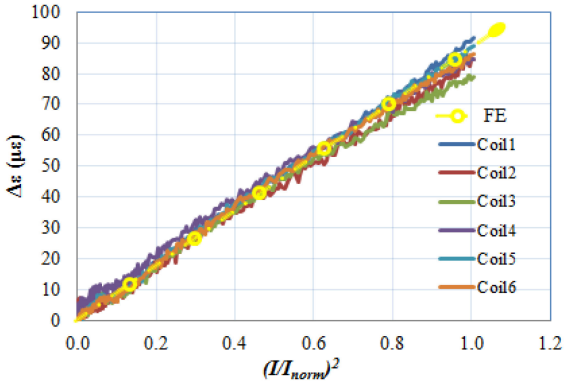

Fig. 13. Measured pole azimuthal strain during the last ramp (451A in sextupoles).

pole strain after cool down could not be measured because strain gauge temperature compensators failed. The magnet behaved as expected in general at room temperature preload and cooldown according to the available mandrel gauge.

V. Mechanical Performance in Quench Tests

The magnet underwent 5 training quenches in sextupoles to reach the maximum currents in solenoids and sextupole (450 A) in the final quench tests.

Pole strain changes during the last ramp are shown in Fig. 13, I_{norm} is the nominal current of the sextupoles. The signals exhibit a linear relation between the pole stress and the Lorentz forces. The FE model results are in agreement with the signals. The linear change of pole stress with the current represents that the pole is gradually unloaded because the poles were initially compressed (absolute pole strains were negative).

According to the experiences gained from other magnets using the "bladder and key" technique, it's generally considered an indication of detachment of the coil from the pole, and in general of low pre-stress if there is a slope reduction or a plateau in the measured pole azimuthal strain during ramps [10], [11]. In the case of FRIB ECR magnet, the measured pole azimuthal strain is linear in general with respect to the Lorentz forces, this is a good sign that the sextupole coils keep under compression to the pole at all times of the operations, and the preload applied at room temperature is considered sufficient.

It is possible to estimate that the average azimuthal compression at the coil/pole interface is about 19 MPa from measured pole strain in Fig. 13. This is slightly less but close to the calculated minimum pre-stress after cooldown shown in Fig. 6. This may indicate that there is still a bit preload margin at the nominal current.

VI. Conclusion

In this paper, we presented the mechanical studies of the FRIB ECR magnet. This magnet features a "shell based" support structure using the "Bladder-and-key" preload concept; and the final tests demonstrate that this structure is capable of applying the required preloads to the sextupole coils. The appropriate preload target was calculated in the FE model. The strain data measured during the room temperature preload operations shows good agreement with the 3D FE results. The final preload was achieved after the magnet was cooled to 4.2 K; the estimated achieved preload is 19 MPa at the pole-turn on sextupole straight section. The pole strain during the current ramp changes linearly with the Lorentz forces in the sextupole coils; therefore, there are no signs of unloading. The FE results are validated by the strain measurements as well.

Acknowledgment

The authors would like to thank warmly Thomas Johnson, Ahmet Pekedis, James Swanson, Joshua Herrera, and Matthew Reynolds for their dedicated work and enthusiasm on this project.

References

[1] C. Taylor *et al.*, "Magnet system for an ECR ion source," *IEEE Trans. Appl. Supercond.*, vol. 10, no. 11, pp. 224–227, Mar. 2000.

[2] G. Machicoane, N. Bultman, G. Morgan, E. Pozdeyev, and X. Rao, "Design status of ECR Ion source and LEBT for FRIB," in *Proc. ECRIS2012*, Sydney, Australia, 2012.

[3] D. Leitner *et al.*, "Status report and recent developments with VENUS," in *Proc. ECRIS*, Chicago, IL, USA, 2008, pp. 1–7.

[4] H. Felice *et al.*, "Design of a superconducting 28 GHz ion source magnet for FRIB using a shell-based support structure," *IEEE Trans. Appl. Supercond.*, vol. 25, no. 3, 2015, Art. no. 4101405.

[5] S. Caspi *et al.*, "The use of pressurized bladders for stress control of superconducting magnets," *IEEE Trans. Appl. Supercond.*, vol. 11, no. 1, pp. 2272–2275, Mar. 2001.

[6] P. Ferracin *et al.*, "Mechanical behavior of HQ01, a Nb_3Sn accelerator-quality quadrupole magnet for the LHC luminosity upgrade," *IEEE Trans. Appl. Supercond.*, vol. 22, no. 3, Jun. 2012, Art. no. 4901804.

[7] H. Pan *et al.*, "Assembly tests of the first Nb_3Sn low-beta quadrupole short model for the Hi-Lumi LHC upgrade," *IEEE Trans. Appl. Supercond.*, vol. 26, no. 4, Jun. 2016, Art. no. 4001705.

[8] E. Rochepault *et al.*, "3-D mechanical analysis of the ECR source magnet for FRIB," *IEEE Trans. Appl. Supercond.*, vol. 25, no. 3, 2015, Art. no. 4100705.

[9] "Metallic Materials and Elements for Aerospace Vehicles Structure," Department of Defense Handbook, Version 5J.

[10] P. Ferracin *et al.*, "Mechanical performance of the LARP Nb_3Sn quadrupole magnet LQS01," *IEEE Trans. Appl. Supercond.*, vol. 21, no. 3, pp. 1683–1687, Jun. 2011.

[11] H. Felice *et al.*, "Test results of TQS03: A LARP shell-based Nb_3Sn quadrupole using 108/127 conductor," *J. Phys. Conf. Ser.*, vol. 234, no. 3, Jun. 2010, Art. no. 032010.